Photothermal therapy of CdTeSe@ZnS quantum dots and their photonic state gain amplification fiber applied to brain gliomas at different stages

Xueqiong Su

nysxq@bjut.edu.cn

Beijing University of Technology

Ruian Zhu

Ningxia Medical University

Yong Pan

Xi'an University of Architecture and Technology

Pengxiang Zhao

Beijing University of Technology

Jin Wang

Beijing University of Technology

Ruimin Wang

Beijing University of Technology

Lishan Yang

Beijing University of Technology

Li Wang

Beijing University of Technology

Wei Zhao

Ningxia Medical University

Zhijun Wang

Ningxia Medical University

Article

Keywords:

Posted Date: March 19th, 2024

DOI: https://doi.org/10.21203/rs.3.rs-4113848/v1

Additional Declarations: There is **NO** Competing Interest.

Photothermal therapy of CdTeSe@ZnS quantum dots and their photonic state gain amplification fiber applied to brain gliomas at different stages

Xueqiong Su[a*], Ruian Zhu[d*], Yong Pan[c*], Pengxiang Zhao[e], Jin Wang[a], Ruimin Wang[a], Lishan Yang[a], Li Wang[a], Wei Zhao[d#], Zhijun Wang[b#]

a The School of Physics and Optoelectronics, Faculty of Science, Beijing University of Technology, Beijing 100124, China
b Department of Radiology, General hospital of Ningxia Medical University, Yinchuan 750004, China
c College of Science, Xi'an University of Architecture and Technology, Xi'an, 710055, China
d Center Laboratory, People's Hospital of Ningxia Hui Autonomous Region, Ningxia Medical University, Yinchuan 750021, China
e College of Chemistry and Life Science, Beijing University of Technology, Beijing 100124, China.

[*] These authors contributed equally: Xueqiong Su, Ruian Zhu and Yong Pan
[#] Address correspondence to Zhijun Wang or Wei Zhao. E-mail: wangzhijun2164@nyfy.com.cn, zhaowei@nxmu.edu.cn

Xueqiong Su nysxq@bjut.edu.cn
Ruian Zhu zhuruian@nxrmyy.com
Yong Pan panyong_paper@126.com
Jin Wang jin.wang@kaust.edu.sa
Pengxiang Zhao zpx@bjut.edu.cn
Ruimin Wang loriawang@emails.bjut.edu.cn
Lishan Yang yanglishan@emails.bjut.edu.cn
Li Wang Lwang.1@bjut.edu.cn
Wei Zhao zhaowei@nxmu.edu.cn
Zhijun Wang wangzhijun2164@nyfy.com.cn

Abstract: Mental nanomaterial-mediated photothermal therapy (PTT) offers a prospective therapeutic strategy for solid tumors. However, its clinical application is limited due to insufficient photothermal conversion efficiency for deep-seated tumor and potential cytotoxic. Few photothermal therapy studies have been reported for tumour cells of different morphologies. In this study, CdTeSe/ZnS quantum dots (QDs) generating photoluminescence at 562 nm and 640 nm under 365 nm excitation are presented. The proliferation activity of RAW264.7 cells phagocytosed QDs exhibited a dose-dependent decline, as expected. *In vitro*, a liquid core fiber loaded with these QDs was utilized for PTT targeting high-grade and low-grade brain glioma cells. In the culture medium of cultured brain glioma cells, the maximum heat around the QDs-fibers under 365 nm laser excitation reached 64.9℃. High-grade U87 glioma cells treated with PTT displayed greater sensitive towards organelle damage compared to low-grade U251 glioma cells. Notably, U87 cells showed significant induction of apoptosis. Therefore, these findings represent further progress towards the applications of QDs-fibers in human solid tumor treatment.

Keywords:

1. Introduction

In recent decades, photothermal therapy (PTT) has shown great promise in the destruction of superficial tumors at a minimally

invasive, micron-level regional scale by utilizing the photothermal conversion effect of light-absorbing materials [1-3]. However, its effectiveness in treating deep tumors is limited due to the insufficient penetration depth of excitation light and energy attenuation impeding effective heat production of photosensitive particles [4-6]. Fortunately, recent advancements in nanoscience have given rise to quantum dots (QDs) with unique photophysical properties that enable enhanced photothermal conversion, which has greatly propelled its application in deep cancer phototherapy. Nevertheless, the selection of photosensitive particles currently encounters challenges due to the presence of cytotoxic elements in ideal photosensitive particles, while bio-friendly particles exhibit limited ability in terms of light transmission and heat generation [6-8]. The cytotoxicity of QDs was assessed in this study using a combination of macrophage phagocytosis assay and cell proliferation activity assay.

In cancer treatment, precise targeting of the tumor is paramount, necessitating consideration of factors such as tumor size, location, adjacent peritumoral stroma, vascular invasion, and other tissue structures to optimize the efficacy of hyperthermia treatment while minimizing damage to healthy tissues [9-11]. The light source should emit sufficient energy to ablate tumor tissue while minimizing damage to adjacent normal tissue, thus precise regulation of thermal damage remains a significant challenge. However, external light sources through normal tissue towards deep-seated lesions often leads to energy attenuation, resulting in reduced therapeutic efficacy. Currently, most advanced photonic agents are typically excited by ultraviolet or visible light and exhibit limited penetration depths (1-3 mm), thereby restricting their application to superficial tumors [12]. Moreover, the presence of chromophores such as hemoglobin within tissues hampers efficient conversion of light energy from photosensitizers [13-15]. Consequently, determining an optimal radiation range for effective tumor eradication remains a complex issue.

This study addresses the two critical questions above by proposing a system for PTT using a liquid core fiber filled with QDs. We aim to achieve a method for tumor cells of different stage of development curing. The QDs, specifically CdTeSe/ZnS, act as optical gain media, and the fiber ring resonator is constructed to achieve a low threshold with a narrow bandwidth and high intensity near-infrared radiation output with ASE. The micro-nano light source device can synchronously transport the near-infrared photothermal reagent to the focal area. The heterogeneity of tumor cells is also a crucial factor affecting the efficacy of PTT [16]. Liquid-core fiber-based PTT was used to treat both high-grade and low-grade glioma cells cultured *in vitro*. The effect difference of PTT on brain glioma cells with different grades was compared using assessing subcellular organelle damage under transmission electron microscopy, and further confirmed the apoptotic effect using flow cytometry analysis. This study provides valuable insights into PTT and establishes a foundation for future applications of photothermal therapy in brain gliomas.

2. Materials and methods

2.1 Preparation of QDs photonic state gain amplification fiber

The aqueous phase method of CdTeSe/ZnS core–shell QDs synthesis was used according to Ref. [17]. The details of QDs including XRD, XPS, TEM and absorption spectrum can be seen in the supporting information (SI) S1-S5. Then, the QDs was filled in a liquid-core optical ring resonator, LCORR (Core diameter is 3 mm, length is 1 m, receiving angle is 60°) for PTT. A fixture like funnel was clamped in a mechanical pump. The QDs solution was poured in the funnel. The mechanical pump was turned on to fill the quantum dot solution into the liquid core fiber.

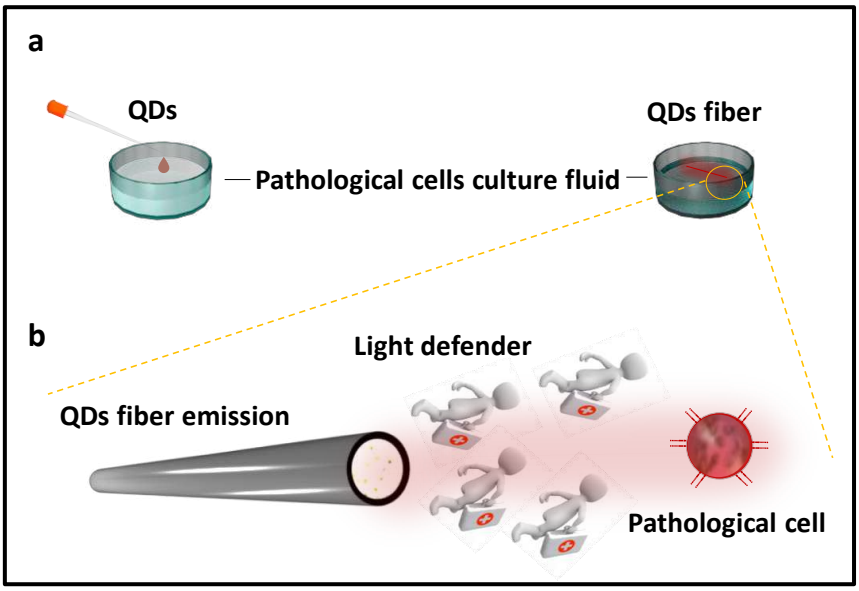

Figure 1 The experiment diagrams. a. Comparative study of cell killing experiment; b. Cell killing diagram.

2.2 Cell culture

The murine macrophage-like cell line RAW264.7, the human glioblastoma multiforme (GBM) cell line U87, and the human glioma cell line U251 were procured from the Institute of Cell Biology, Chinese Academy of Sciences (Shanghai). The RAW264.7 cells were cultured in Dulbecco's modified Eagle's medium (DMEM, Biological Industries, #C3101-0500) supplemented with 10% newborn calf serum (NBCS, Gibco, # 16010159). U87 and U251 cells were cultured in DMEM supplemented with 10% fetal bovine serum (FBS, Mema, # YSN1121). All cells were maintained at 37˚C under a 5% CO_2 atmosphere.

2.3 Cytotoxic effects of QDs on RAW264.7 cells using CCK8 assay

RAW264.7 cells cultured in 24-well plates were treated with three types of QDs at varying concentrations (1.7×10^{-4} M, 8.5×10^{-5} M, 4.25×10^{-5} M, 2.125×10^{-5} M, and 1.0625×10^{-5} M) for 48h. The culture medium was discarded, followed by PBS washing to remove unswallowed QDs. The phagocytosis of QDs by RAW264.7 cells was confirmed using near-infrared fluorescence imaging at 680 nm under a fluorescence microscope. Furthermore, the cytotoxicity of QDs on RAW264.7 cells was evaluated using the tetrazolium salt-based CCK-8 cell counting assay (Keygenbiotech, #KGA9305-500). In detail, following QDs at various concentrations (0 μM, 3 μM, 10 μM, 30 μM, 100 μM, 300 μM) to cells cultured in 96-well plate for 24 h, the culture medium was subsequently replaced with a CCK-8 working solution. The absorbance of samples at 450 nm was read using iMark™ Microplate Absorbance Reader (Biorad, # 1681135).

2.4 Effect of QDs-fibers under UVA excitation on organelle structure of tumor cells using a transmission electron microscope

After loading QDs into multiple 50 μL capillaries, their ends were sealed with Vaseline gel to fabricate liquid core fibers containing QDs. Subsequently, these fibers were adhered and arranged onto cell culture plates at specific intervals. U251 and U87 cells were respectively seeded onto these plates and incubated overnight. To assess the impact of PTT on organelle structures, the cells were exposed to a UV lamp positioned approximately 20 cm above them for 4 minutes. The tumor cells were collected after 6 h, 12 h, and 24 h of incubation for TEM. Sample preparation and TEM detection were conducted by Servicebio Technology Co., Ltd. (Wuhan, China).

2.5 Effect of QDs-fibers under UVA excitation on tumor cell apoptosis

The QDs-fibers were prepared following the method outlined in section 2.4. For the apoptosis assay, cells were exposed to radiation for durations of 0 min, 1 min, 2 min, and 4 min before being collected after 12 h. The Annexin V-AbFluor™ 488/PI

Apoptosis Detection kit (Abbkine, # KTA0002) was used for cell staining, and apoptosis analysis was conducted using the BD Accuri™ C6 Plus Flow Cytometer (BD Biosciences, USA). Experimental data were analyzed utilizing the FlowJo software (Treestar, USA).

2.6 Analysis of Optical Characterization

The PL of QDs was measured using a NIR512 and S2000 spectrograph. Photothermal radiometry was detected using the Cytation 5 cell imaging microplate detection system. Dead cell images were obtained using a FLUKE device. The results of ablation were tested using Geminin SEM 300. Transient absorption (TA) spectra were conducted using a femtosecond laser with a pulse width of 150 fs and repetition rate of 5 kHz form Spectra-Physics. The surface morphology of $CsPbBr_3$ QDs and cytoplasm was analyzed using scanning electron microscopy (SEM, JEOL JSM 6500F). X-ray diffraction (XRD) spectrum on QDs structures were measured with a Bruker D8 Advance instrument. The absorption spectrum of the device was determined using a Hitachi U-4100 spectrometer. Raman spectra (Raman, BWTEK BTR113-785-BAC102, instrument model) were tested without.

3. Result and discussion

To track the killing of glioma cells using quantum dots, we selected phagocyte RAW264.7 due to its strong phagocytosis ability to combine with quantum dots first. The TEM image with of scale of 50, 20, 10, 5 nm of CdTeSe/ZnS core–shell QDs and CdTeSe/ZnS@SiO_2 are presented in the **figure 2a**. The purpose of incorporating SiO_2-coated quantum dots in this paper is for the bio-friendliness of the QDs material. The phagocytosis ability of RAW264.7 to combine with quantum dots will allow quantum dots to demonstrate their tracing ability in phagocytes, which can then be extended to other cells. Phagocytosis will occur after the quantum dots are dropped into the phagocyte solution. The process of phagocytosis begins as the quantum dot approaches and is adsorbed to the edge of the phagocyte. The process of phagocytosis begins as the quantum dot approaches and is adsorbed to the edge of the phagocyte. The process of phagocytosis begins as the quantum dot approaches and is adsorbed to the edge of the phagocyte. The phagocyte then engulfs the quantum dot and digests it, producing exosomes that contain a portion of the quantum dot. The process of phagocytosis begins as the quantum dot approaches and is adsorbed to the edge of the phagocyte. These exosomes eventually separate from the phagocyte, as seen in **figure 2b** and **2c**.

The ability to cross the blood-brain barrier (BBB) is a crucial factor affecting the delivery and effectiveness of medicinal therapies for brain tumours. Our study employed an exosomes (Exos) encapsulation method to produce MNLs, possessing both a random laser structure and the BBB crossing ability. Exos are natural bio-nanovesicles with membrane structure, effectively secreted by living cells, characterized by low immunogenicity, and capable of efficiently permeating various physiological barriers like the BBB to serve as effective drug delivery vehicles [18]. To incorporate both MNPs and QDs into Exos, we selected mouse macrophage RAW264.7 as the parental cell for Exos production due to its powerful phagocytic ability. Firstly, the MNPs and QDs were phagocytosed by RAW264.7 cells, and subsequently, the Exos-MNPs-QDs complex was formed through the secretion of Exos. Phagocytosis of RAW264.7 cells co-cultured with and without quantum dots for 48 hours are presented in the **figure 2d-f**. Figure 3d provides the phagocytosis analysis of the cell culture solution in the absence of quantum dot addition. It is evident from the figure that phagocytosis is absent. When CdTe@CdSe quantum dot was added to the co-cultured culture solution with phagocytes, red-labelled fluorescence became apparent upon irradiation with UV light. This indicates that a considerable amount of quantum dots has effectively engulfed the cell [19-21]. Next, the culture solution was substituted with a new QDs-CdTe@CdSe@SiO_2. However, there is no discernible phagocytosis observed. No clear phagocytosis has been observed. Two possible reasons could lead to this phenomenon. Firstly, the fluorescence intensity of quantum dots enclosed in SiO_2 is lowered due to reflection of both excitation light and fluorescence by it. The second reason is attributed to the enlargement in both the volume and surface area of one quantum dot that is encapsulated by SiO_2, subsequently leading to phagocytosis. Once uptake occurs, these particles can be readily supported, ultimately resulting in cell death. Therefore, we performed quantum dot optimization experiments. The details of process with TEM expression can be seen SI 6-8.

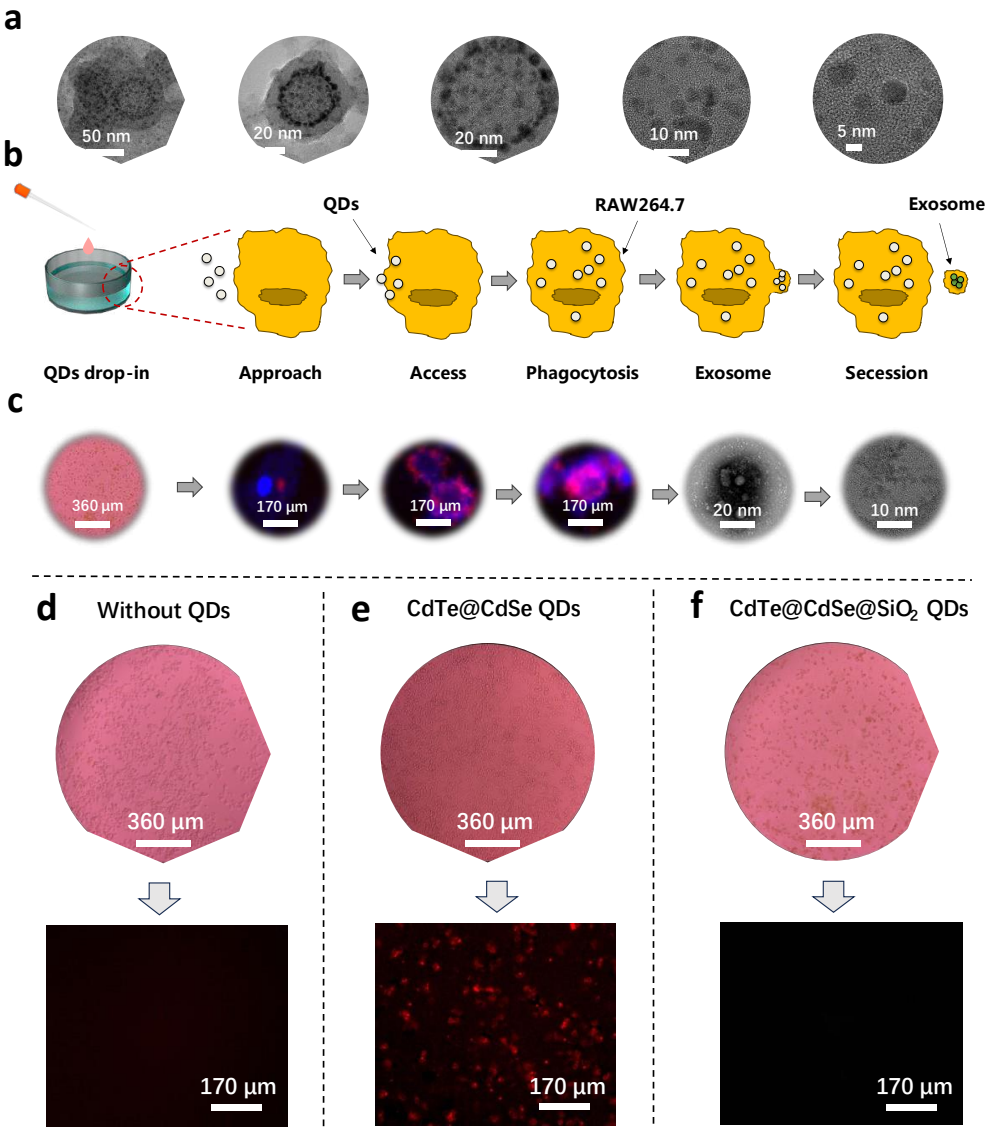

Figure 2. Schematic diagram of a quantum dot being phagocytosed. **a** TEM images of the CdTeSe/ZnS@SiO_2. **b** Phagocytosis schematic. **c** Process of phagocytosis in RAW264.7 cells**. d-f** QD could be successfully absorbed into the RAW264.7 cells under light microscope (Scale bar, 360 μm) and immunofluorescence detection (Scale bar, 170 μm).

3.1 The phagocytosis and cytotoxicity effects of QDs materials on RAW264.7 cells exhibit significant variations.

The macrophage-like cell line RAW264.7 has been widely recognized as a suitable model for studying macrophages due to its capability of performing phagocytosis, making it an ideal model for evaluating the biological effects of QDs on cells. Although QDs have been extensively utilized in biological research, they may also induce adverse reactions such as toxicity. In this study, we observed that the ingestion of No.1 QDs (CdTe@CdSe) by RAW264.7 cells resulted in substantial cell debris surrounding the dots despite their strong luminescence (**Figure 3 a_1-e_1**), which is consistent with previous findings. To enhance the biocompatibility of QDs, SiO_2-coated QDs (No.2 and No.3) were employed in our experiments, which led to reduced cell debris but weaker luminescence compared to No.1 QDs due to their physical properties **(Figure 3 a_2-e_2, a_3-e_3)**. In addition, when comparing equal concentrations, RAW264 .7 was found to internalize more No.1 QDs than other types of QDs, indicating that RAW264.7 exhibits a size-dependent absorption pattern. To further investigate the cytotoxic effects of QDs, we conducted CCK8 assays **(Figure 3 f-h)**. Notably, No.3 QDs exhibited less cytotoxicity (IC50=10.66μmol/L) compared to No.l QD s (IC50=8.822 μmol/L), possibly attributed to the appropriate thickness of the SiO_2 layer encapsulation. However, No.2 QDs coated with SiO_2 did not demonstrate excellent biocompatibility (IC50 =6.921μmol/L). These data suggest that further optimization is required for better application of QDs in biotherapy.

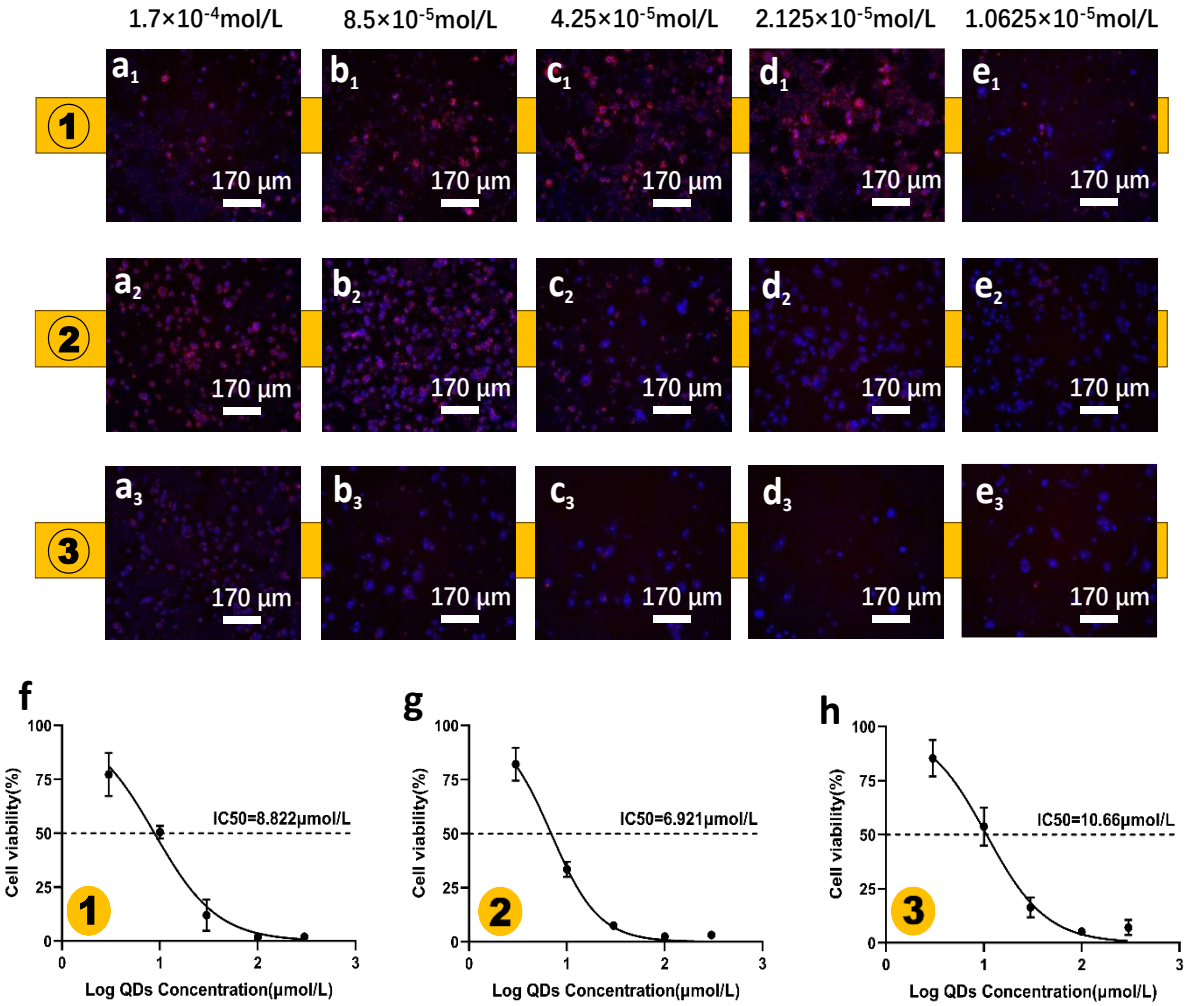

Figure 3. The toxicity of QDs on RAW264.7 cells and their impact on phagocytosis by RAW264.7 cells. **a1-c3** Immunofluorescence images of QDs (red) in RAW264.7 cells (representative image from three repeats). Nuclei were labeled with DAPI (blue). Scale bar, 170 μm. **a1-e1** ① CdTe@CdSe, solvent: water, **a2-e2** ② CdTe@CdSe@SiO_2, 50 μL of TEOS preparation, solvent: water, **a3-e3** ③ CdTe@CdSe@SiO_2, 100 μL of TEOS preparation, solvent: water. **f-h** IC50 of QDs in RAW264.7 cells. RAW264.7 cells were treated with QDs concentrations varied from 0 to 300 μM for 24 h and analyzed using CCK8. IC50 represents the concentration of QDs that caused a 50% reduction in the number of treated cells compared to the untreated control. n = 3 biological replicates.

3.2 Under UVA excitation, Characterization of photothermal effects of QDs and induced significant structural damage to cells

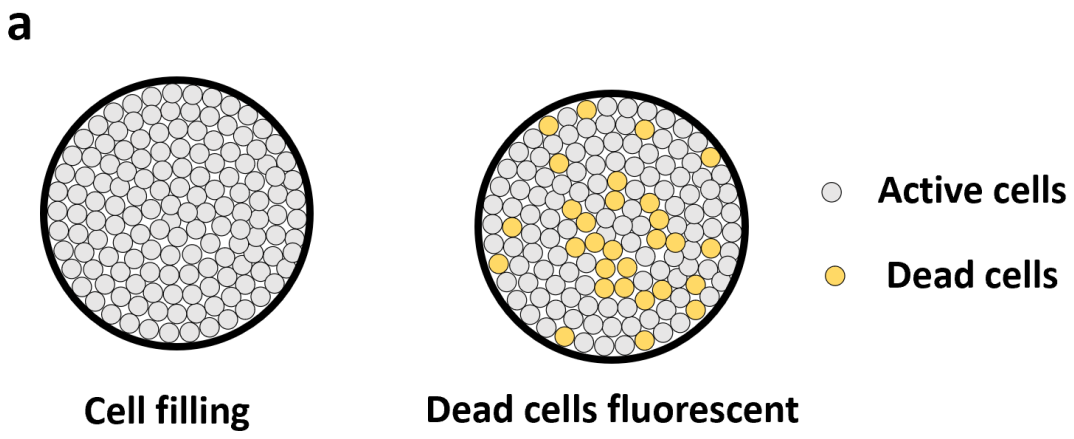

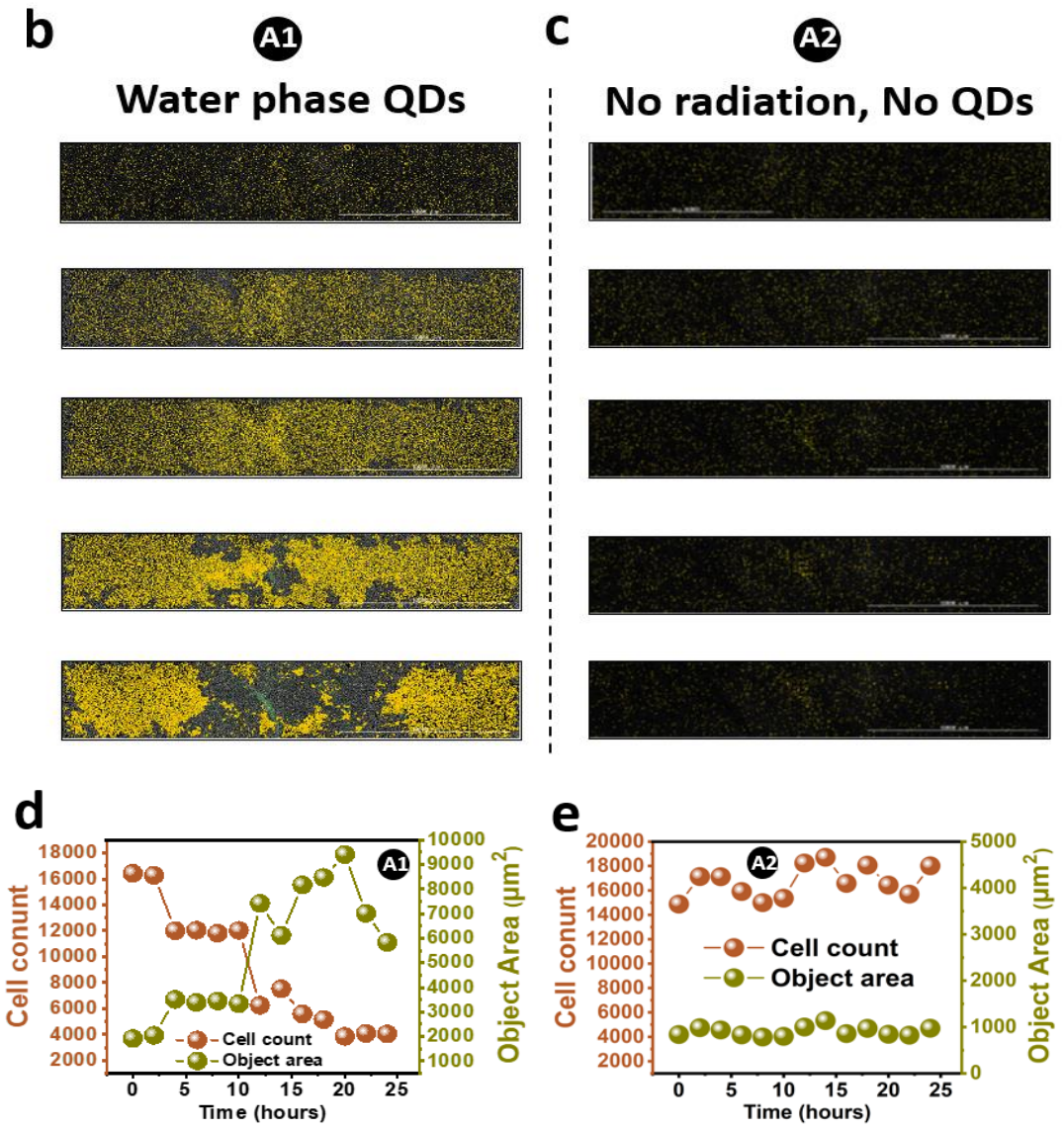

Figure 4. Cell death rate in all experiment group. **a**-Operation process of cell killing; **b**-A1: Water phase QDs; **c**-A2: No QDs and excitation; **d**-The relationship between cell count, object area and time of A1; **e**-The relationship between cell count, object area and time of A2. The yellow area is the dead cells. The cell count is number of viable liver cancer cells. The object area is the proportion of dead cells.

To prove the killing effect of photothermal radiation on cells, fluorescence microscope was used to characterize the death of cells in the culture medium. Operation process of cell killing can be seen in **figure 4a**. The cells were spread all over the petri dish for accurately measuring mortality. The cells had been injected with fluorescent agent before they are placed in the petri dish. Then, QDs fiber was added in the cells. The cells began to be killed after the fiber was excited. Finally, dead cells produce white light due to the action of fluorescent agents. Therefore, the area of fluorescence can be used as a basis for judging mortality. To clarify the killing ability of quantum dot fiber more accurately, Viability assay (VA) experiments were carried out. For water phase QDs, cell count and object area show a stepped upward trend in range of 3-10 and 12-24 hours (**figure 4b, A1 group**). This suggests that the killing ability of water phase QDs is weaker **(figure 4d)**. The results shown in **figure 4c (A2 group)** are the experimental results of the control group, which proves the killing effect of QDs on liver cancer cells (**figure 4e)**.

3.3 Under UVA excitation, Characterization of photothermal effects of QDs fiber

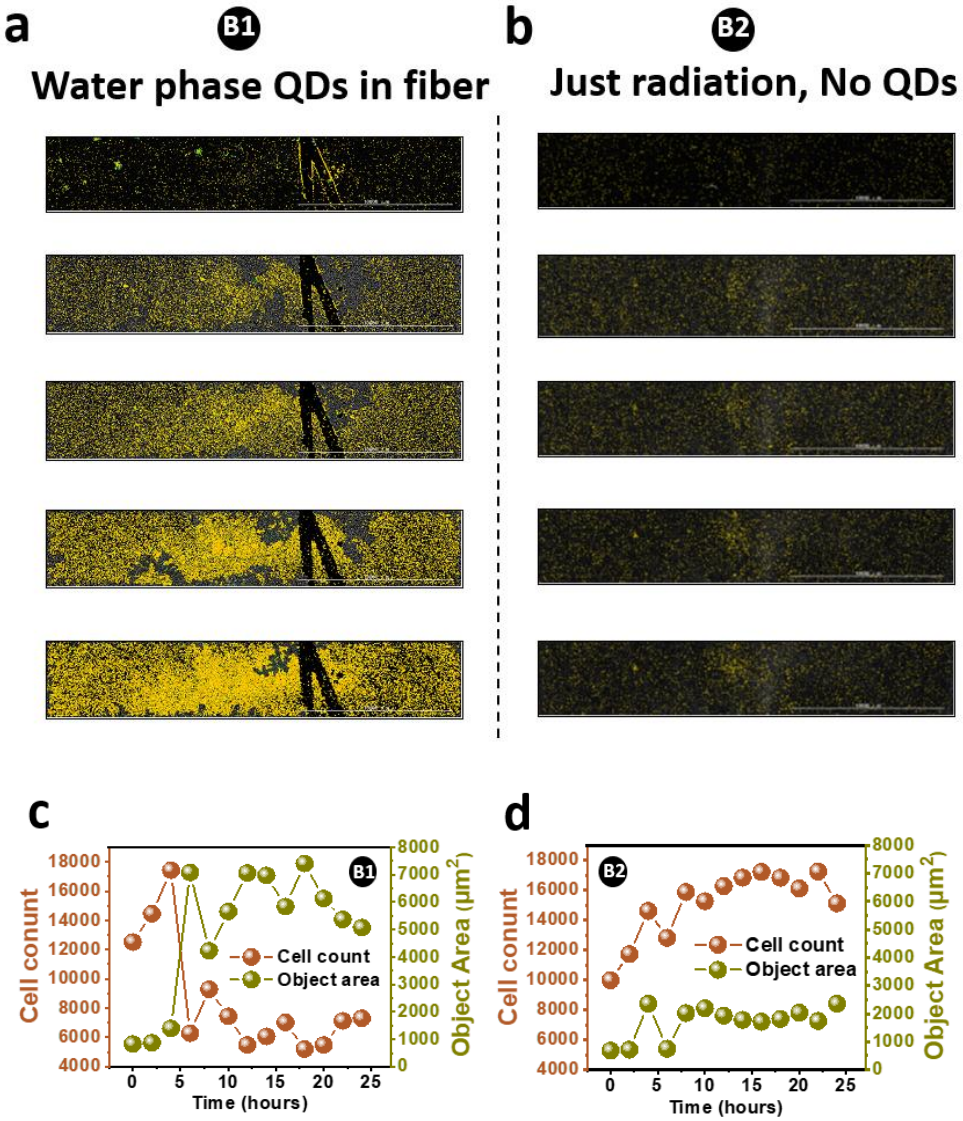

Figure 5. Cell death rate in all experiment group. **a**-Water phase QDs in fiber; **b**-Just excitation. **c**-The relationship between cell count, object area and time of A1; **d**-The relationship between cell count, object area and time of A2. The yellow area is the dead cells. The cell count is number of viable liver cancer cells. The object area is the proportion of dead cells.

The experiment of QDs in fiber are presented (**figure 5, B1-B2 group**). For water phase QDs in fiber, the traces left by the optical fiber are obvious (**figure 5a and 5b**). Both cell count and object area show a fluctuating trend. It is noted that there is little difference in the killing ability for liver cancer cells with water-based QDs filling in fibers (**figure 5c and 5d**). The reason for this phenomenon can be explained by positioning function of fiber. QDs without fiber will be continuously diffused after being dropped into the cell dish, and they will be diffused randomly. Their advantages are strong killing strength, but their disadvantages are that they cannot be accurately located ability. On the contrary, the main radiation area of fiber is around its core, which has strong positioning characteristics.

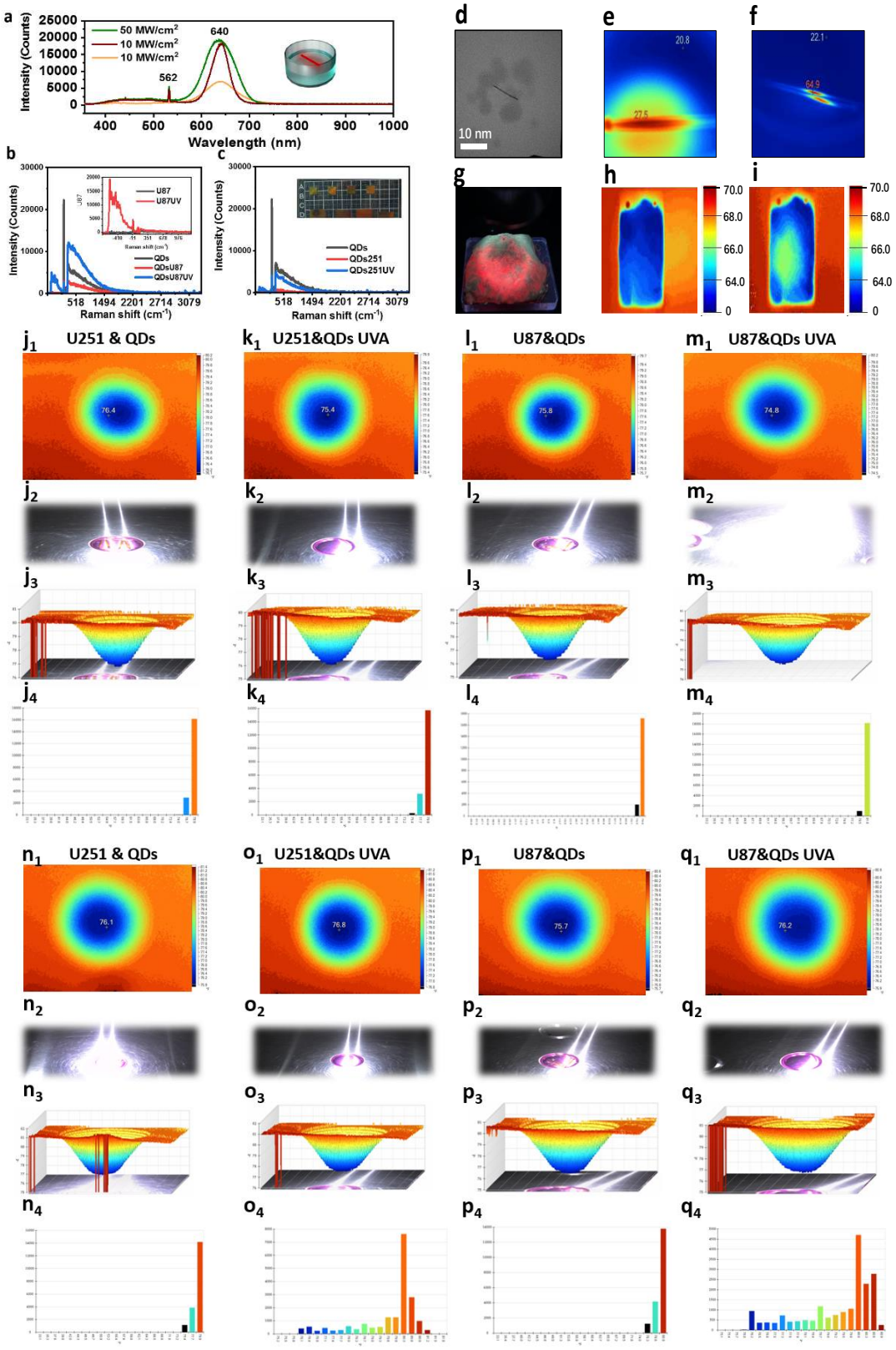

Figure 6. The PL spectrum, Raman spectrum, TEM image, photothermal radiometry (PTR) spectrum exciting at room temperature. **a**-The PL spectrum of QDs fiber in solution; **b**-The Raman spectrum of the QDs with U87 cells, the inset is the amplified spectrum around -410cm^{-1}; **c**-The Raman spectrum of the QDs with U251 cells, enhanced Raman testing sample photography; **d**-The TEM image of the QDs; **e-f** PTR spectrum in solution of the QDs fiber; **g**-The photograph of chicken liver drops after the application of quantum dots; **h**-Pre-illumination infrared imaging; **i**-Infrared imaging image after 20 min of illumination. j-m PTR, IR-photo, 3D-PTR, histogram of U251 6h QDs, U251 6h UVA, U87 6h QDs, U87 6h UVA before light, respectively; j-m PTR, IR-photo, 3D-PTR, histogram of U251 6h QDs, U251 6h UVA, U87 6h QDs, U87 6h UVA before light, respectively; n-q PTR, IR-photo, 3D-PTR, histogram of U251 6h QDs, U251 6h UVA, U87 6h QDs, U87 6h UVA before light, respectively; j-m PTR, IR-photo, 3D-PTR, histogram of U251 6h QDs, U251 6h UVA, U87 6h QDs, U87 6h UVA after light, respectively.

The PL spectrum of QDs fiber is shown in **figure 6a**. The PL of 640 nm was observed firstly in CdTeSe/ZnS QDs fiber excited by 365 nm UV light in the solution. This means that QDs fiber can be used as killing source for liver cancer cells (killing sensitive band in range of 600-1500 nm [22,23]). Besides, the laser peak at 562 nm was also detected excited by 365 nm UV light. This laser contributes thermal radiation energy although 562 nm not in the kill sensitive band. The Raman spectrum of the QDs with U87 cells can be seen in the **figure 6b**. The Raman peak at position 268 cm^{-1} was observed in the spectra of both sets of samples, which consisted of quantum dots and quantum dots & U87 cells without light exposure. This peak can be attributed to the Raman phonon vibrational peaks of the quantum dots [24]. However, the Raman spectra of quantum dots and U87 exhibit Raman peaks under UV illumination, including the 268 cm^{-1} Raman peak and the anti-Stokes peak at -573.5 cm^{-1}(The inset sepctrum). A change in the ratio of the positive Stokes Raman peak area to the anti-Stokes Raman peak area indicates a direct photothermal effect [25], which is caused by the excitation of quantum dots by UV light in U87 cells. The coexistence of quantum dots with U251 cells in the sample is similar to the previous situation, except for a weaker intensity of the anti-Stokes peak (**figure 6c**). However, the ratio of the positive Stokes Raman peak area to the anti-Stokes Raman peak area still changed, which proves the photothermal effect of quantum dots with U251 cells. The TEM image of CdTeSe/ZnS QDs can be seen in the **figure 6d**. The average size of QDs is 6.6 nm according to the size statistic. To demonstrate the thermal effect of quantum dot optics, we first measured the thermal radiation emitted after being excited in solution. The PL radiation energy was measured to calibrate energy data. The temperature around the optical fiber reaches 27.5℃ (**figure 6e**). Then, the fiber was rotated in the solution for averaging heat and energy. Furthermore, the heat generated by QDs fiber are also increasing 64.9℃ (**figure 6f**) as growth of time, respectively. These results confirm that quantum dot optical fibres exhibit thermal radiation and thermal influence on the surrounding environment when excited. To confirm the influence of this thermal effect on cells, quantum dots were coated onto chicken livers and tested for their thermal effect [26, 27]. The photograph of chicken liver drops after the application of quantum dots can be seen in the **figure 6g**. Prior to excitation of the quantum dots, thermal testing revealed no relevant thermal radiation was generated and the quantum dots did not have a thermal impact on the chicken liver cells (**figure 6h**). Upon excitation of the quantum dots, the test results revealed the generation of relevant thermal radiation, indicating that the chicken liver cells were not thermally affected (**figure 6i**). Both thermal radiation tests in this section demonstrate that quantum dots, when excited, are capable of having a certain thermal impact not only on their surroundings but also on biological cells.

To further illustrate the photothermal effect of QDs, PTR, IR-photo, 3D-PTR and histograms of four sets of control samples mixed with U87 and U251 before and after light exposure are provided. Before light exposure, four sets of samples were analyzed: U251&QDs, U251&QDs with UVA, U87&QDs, and U87&QDs with UVA (**figure 6j-m**). The disparity among the PTR plots of the four sample groups is minimal, resulting in insignificant differences in their 3D unfolded plots (with vertical coordinates in °F) and histograms. The inclusion of the unilluminated group serves the primary purpose of comparison. The photothermal assay was repeated after each group of samples had been exposed to light for 6 hours. Analysis of the four sets of photothermal effect data revealed that U251&QDs with UVA and U87&QDs with UVA exhibited different ranges of photothermal effects (**figure 6o_4 and q_4**), which is consist with the results of Raman spectrum. This finding demonstrates that the photothermal properties of quantum dots in contact with U251 and U87 cells can be directly observed, particularly after excitation, and that the photothermal region is enlarged. The details of infrared of illumination with PTR, IR-photo, 3D-PTR, histogram of U251 and U87 can be seen in SI 9-16.

3.4 Under UVA excitation, QDs-fibers induced significant structural damage to organelles in GBM cells

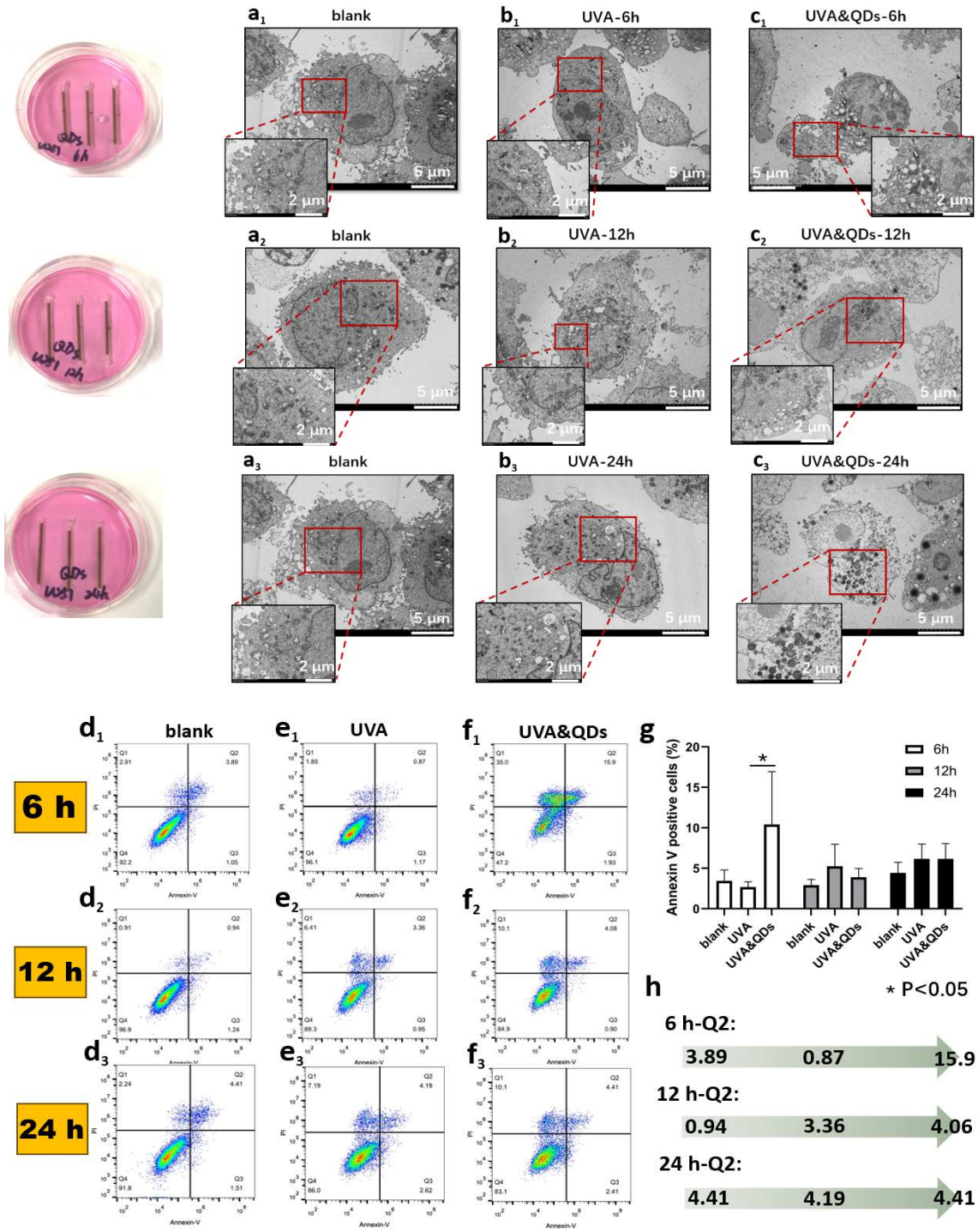

Figure 7. Transmission electron microscopy to detect organelle changes in U251 cells. **a**$_{1\text{-}3}$ Blank control group; **b**$_{1\text{-}3}$ UVA-12 h; **c**$_{1\text{-}3}$ UVA&QDs-12 h. The photograph on the left shows an experiment with a quantum dot photonic state gain amplification fiber in U251 brain glioma solution. The inset in lower left corner is the schema of the three region (i, j, k) around the quantum dot photonic state gain amplification fiber. The highlighted section indicates where the cell was destroyed. The flow cytometry to detect the effect of photothermal effect of QDs on glioma cell survival of U251: **d**$_{1\text{-}3}$ Blank control group; **e**$_{1\text{-}3}$ UVA-12 h; **f**$_{1\text{-}3}$ UVA-24 h. The Q1 region displays PI positivity, indicating cells that have undergone necrosis and have been lost the most. The Q2 region shows full positivity, indicating late apoptotic cells where the nucleus begins to ectopically turn over. The Q3 region represents AV-positive PI-negative cells in early apoptosis, where only the cell membrane is ectopically turned over. The Q4 region represents live cells with no apoptotic percentage of cells, and both dyes are negative and unbound; **g** Statistical data plotted in Q1+Q2 for the three samples irradiated at different times; **h** Statistical data plotted in Q2 for the three samples irradiated at different times.

To enhance PTT efficacy, mitigate the cytotoxicity of QDs, and prevent QD dispersion, we developed QDs-fibers for PTT on human brain tumor cells (Fig. 5, left). UVA+QDs group, and the QDs glass capillary rows were fixed at the bottom of the cell

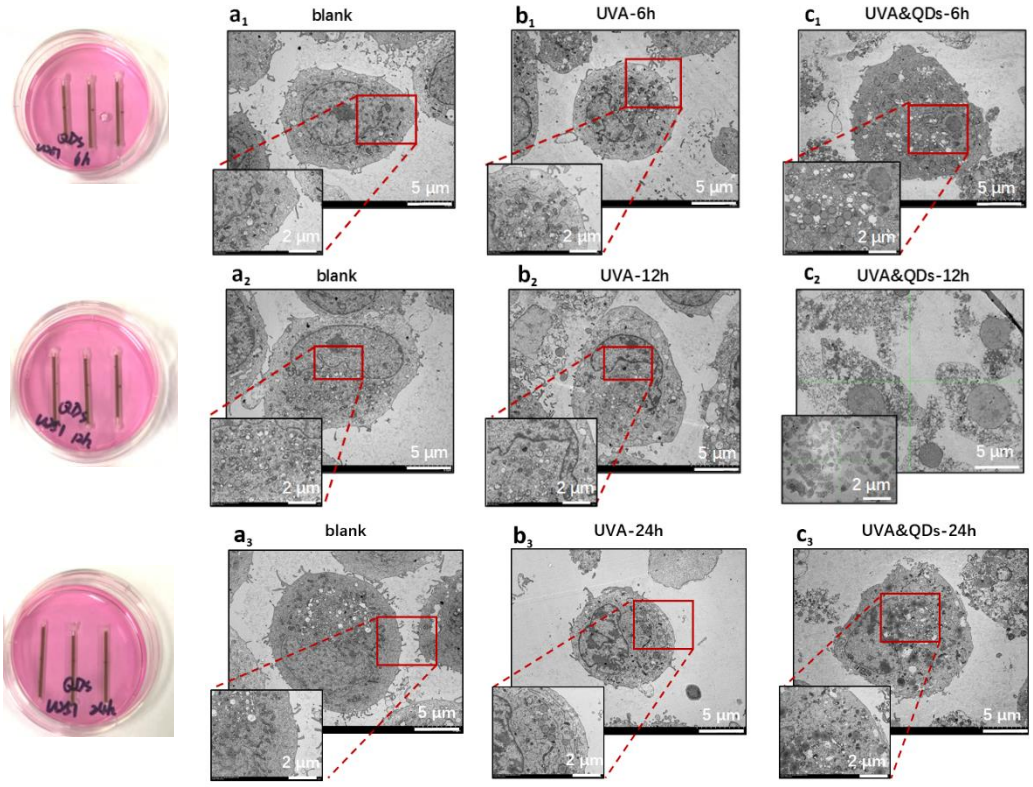

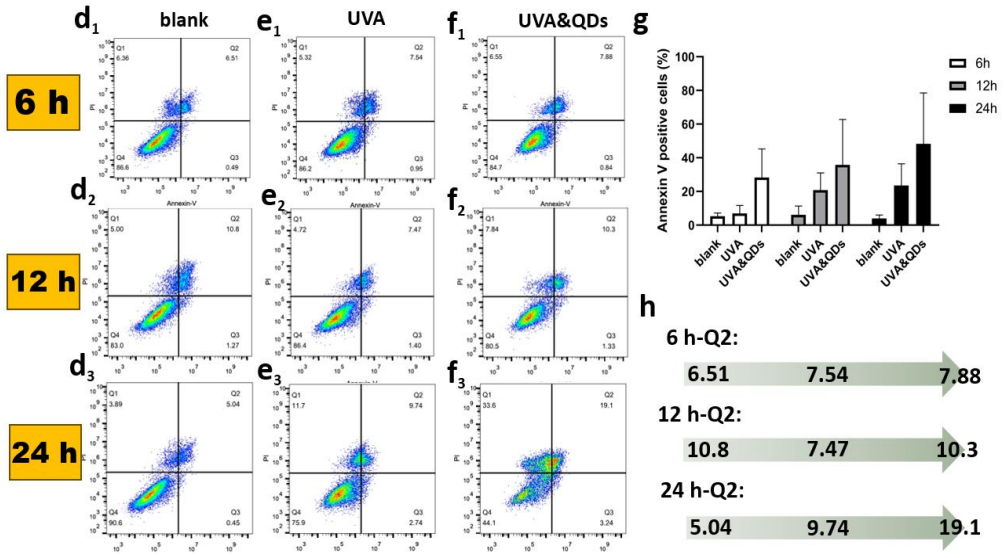

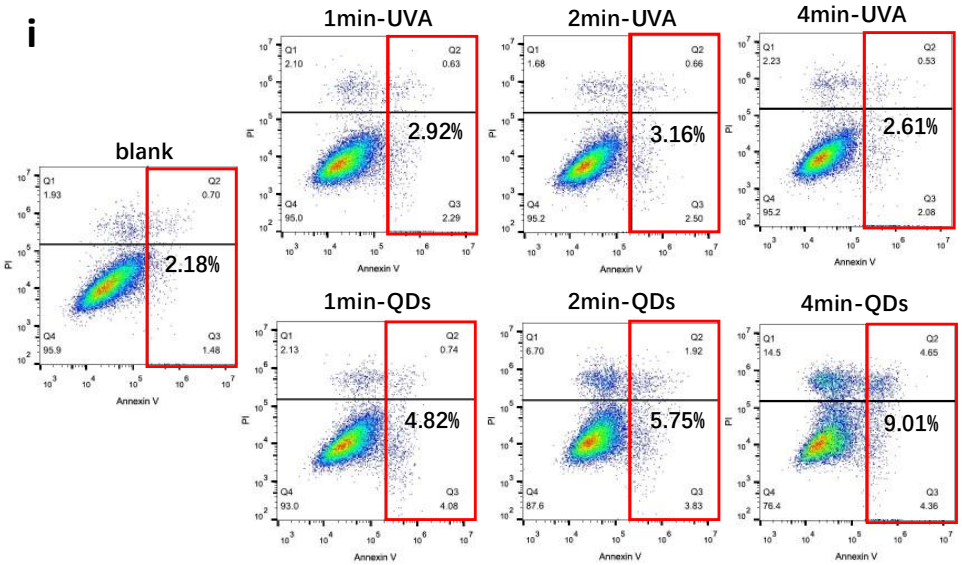

Figure 8. Transmission electron microscopy to detect organelle changes in U87 cells. a_{1-3} Blank control group; b_{1-3} UVA-12 h; c_{1-3} UVA-24 h. The photograph on the left shows an experiment with a quantum dot photonic state gain amplification fiber in U87 brain glioma solution. The inset in lower left corner is the schema of the three region (i, j, k) around the quantum dot photonic state gain amplification fiber. The highlighted section indicates where the cell was destroyed. d_{1-3} Blank control group; The flow cytometry to detect the effect of photothermal effect of QDs on glioma cell survival of U87: e_{1-3} UVA-12 h; f_{1-3} UVA-24 h. The Q1 region displays PI positivity, indicating cells that have undergone necrosis and have been lost the most. The Q2 region shows full positivity, indicating late apoptotic cells where the nucleus begins to ectopically turn over. The Q3 region represents AV-positive PI-negative cells in early apoptosis, where only the cell membrane is ectopically turned over. The Q4 region represents live cells with no apoptotic percentage of cells, and both dyes are negative and unbound. **g** Statistical data plotted in Q1+Q2 for the three samples irradiated at different times; **h** Statistical data plotted in Q2 for the three samples irradiated at different times; **i** The change for U87 apoptotic cell rates with QDs-fibers-based PTT treatment (representative image from three repeats). Apoptosis analysis was measured by flow cytometry of U87 cells at 12 h after different UVA excitation times (0 min, 1 min, 2 min, 4 min). The red boxed area (Q2+Q3) indicates apoptotic cells.

culture dish, while the blank control group and UVA irradiation group (PTT-treated group) were set up. After 6 hours of irradiation, the cellular structure of the blank control group remained intact, with abundant mitochondria (**figure 7a$_1$**). Only the UVA-irradiated group showed chromatin margination (**figure 7b$_2$**). In the UVA+quantum dot group, chromatin continued to marginate, the nuclei of the cells were divided, and the number of vacuoles in the cytoplasm increased (**figure 7c$_3$**). After 12 hours of irradiation, the cellular structure of the blank control group remained intact, with abundant mitochondria. Only the UVA-irradiated group showed chromatin margination and nuclear division. In the UVA+quantum dot group, chromatin continued to marginate, nuclei were divided, and the number of cytoplasmic vacuoles increased. After 24 hours of irradiation, the cellular structure of the blank control group remained intact, with abundant mitochondria [28, 29]. However, in the UVA-irradiated group, chromatin edge aggregation, lysosomes in the cytoplasm, and mitochondrial swelling were observed. In the UVA+quantum dots group, the nuclear membrane was incomplete, lysosomes appeared abundantly in the cytoplasm, and organelles disappeared. It can be noticed from the three regions of i,j,k that cells are killed at a higher rate around the quantum dot fiber.

Flow cytometry was used to detect the effect of PTT on the survival of glioma cells U251. As shown in **figure 7d-f**, UVA irradiation alone did not have a significant effect on cell survival, which was approximately 95%. However, when UVA irradiation was given after placing the QDs capillaries, the survival rate decreased to 85% compared to the blank control group. After 6 hours, the proportion of apoptosis increased to 6.68% and the proportion of necrosis increased to 6.64%. Additionally, the 24-hour survival rate decreased to 73.8%, with the percentage of apoptosis increasing to 7.73% and the percentage of necrosis increasing to 17.9% (figure 7d$_2$). These findings suggest that QD-based photothermal therapy can decrease the survival rate of U251 glioma cells. Comparison of longitudinal data showed that UVA$QDs for U251 produced a higher killing rate after 6h of radiation. the increased regeneration rate of the cells after 12h and 24h also illustrated the effect of quantum dots on U251 toxicity cell killing. The experimental group exposed to 6 hours of light with QDs & UVA showed the highest data from the annexin V positive cells counted in the Q1+Q2 region (**figure 7g**). This suggests that for U251 cells, 6 hours of light exposure has the highest QDs&UVA killing power. Subsequently, the Q4 values in the other control groups increased over time (from 6 h to 12 h), and the Q2 values also changed to varying degrees. After 6 hours of light exposure, the photothermal effect of quantum dots killed some U251 cells, followed by a sudden increase in the rate of new cell production. However, the killing effect continued to decrease and eventually, after 24 hours, many new U251 cells were reanimated. The longitudinal comparison in **figure 7h** shows that the value of Q2 did not change significantly.

The transmission electron microscopy to detect organelle changes in U87 cells can be seen in **figure 8**. For the 6-hour irradiation, the cellular structure was basically intact in the blank control group. Only in the UVA-irradiated group, chromatin edge aggregation, nuclear deformation and lysosomes in the cytoplasm could be observed, while in the UVA+quantum dot group, nuclear deformation, a large number of lysosomes and vacuoles in the cytoplasm, and disappearance of organelles could be observed. For the 12-hour irradiation, the cell structure of the blank control group was basically intact. Only in the UVA-irradiated group, chromatin edge aggregation, nuclear deformation and lysosomes in the cytoplasm could be observed, and a large number of cells were necrotic in the field of view of the UVA+quantum dot group. For the 24-hour irradiation, the cell structure of the blank control group was basically intact. Only in the UVA-irradiated group, chromatin edge aggregation, nuclear deformation, and lysosomes in the cytoplasm could be observed. nuclear deformation, and a large number of

lysosomes and vacuoles in the cytoplasm could be observed in the UVA+quantum dots experimental group. UVA+quantum dots group showed nuclear deformation and a large number of lysosomes and vacuoles in cytoplasm. It also can be noticed from the three regions of (i, j, k) that cells are killed at a higher rate around the quantum dot fiber.

Flow cytometry was used to detect the effect of PTT on the survival of glioma cells U87 (**figure 8d-f**). The thermal impact of quantum dots on the U87 is noticeable. For the cases detected after 6 and 12 hours, there was not a significant difference in the cell death rate of glioma cells between the three scenarios of blank, UVA, and UVA&QDs. The difference in data for Q1 was 0.19 and 1.84. However, 24 hours later, a significant number of dead cells were detected, with Q2 and Q3 values reaching 33.6 and 19.1, respectively. This confirms that quantum dots have a significant killing effect on U87 cells, with the number of dead cells being 3.3 and 4.5 times higher than that of U251 cells. Furthermore, the regeneration of cells after killing was greatly inhibited, indicating the lethal effect of quantum dots on cells [30]. The experimental group with 24 hours of light exposure to QDs&UVA had the highest QDs&UVA kill for U87 cells, as evidenced by the cells counted in the Q1+Q2 region (**figure 8g**). This finding contrasts with the results for U251 cells combined with quantum dots. The Q4 values in the experimental group, exposed to 24 hours of light with QDs&UVA, decreased from 84.7 to 44.1, while the values of Q4 in the other control groups were increasing. Additionally, the values of Q1 and Q2 were increasing. The longitudinal comparison in **figure 8h** shows an increase in the value of Q2 from 7.88 to 19.1. These results suggest that the photothermal effect of quantum dots has a significant killing effect on U87 cells, with greater toxicity and intensity [31].

Considering the detrimental impact of PTT based on QD-fibers on glioma cell organelles and bio-membranes, it is reasonable to speculate that these damaged cells may experience delayed apoptosis. To validate this inference, we employed flow cytometry to assess the apoptosis of U87 cells 24 hours post-PPT treatment. Our findings revealed a significant increase in the proportion of apoptotic U87 cells cultured in QDs-fiber culture dishes with prolonged excitation time of low-dose UVA compared to both the low-dose UVA alone group and the blank control group (**Figure 8i**). Previous studies have demonstrated that tumor cells, being immature proliferative cells, exhibit lower tolerance towards temperature elevation than normal cells. Elevated temperatures can enhance bio-membrane permeability, protein extravasation, and chromatin structure alterations. Apoptosis can be induced when temperatures exceed 41 ℃. In this study, local temperature within QDS-fiber could reach up to 49℃ upon receiving UVA excitation. As anticipated, with longer excitation time of a low-dose of UVA, the thermal effect exerted by QDs-fiber persisted for an extended duration leading to increased apoptosis rates. However, it is crucial to control radiation time within an appropriate range to prevent potential damage caused by UVA exposure. The statistical data of Q1-Q4 of flow cytometry detecting on U251 and U87 can be seen in SI 17-24. The ASE of CdTeSe/ZnS QDs photonic state gain amplification fiber can be seen SI 25.

4. Conclusion

In summary, this study aims to combine optoelectronic technology with biomedical technology by using BG-targeting cyclic peptide RGD4C-modified Exos as a carrier to load and wrap rare earth element-doped CdTeSe/ZnS and CdTeSe/ZnS@SiO_2 sulfur-based bilayer core-shell QDs. The photonic state gain amplification fiber for QDs is designed to cross the BBB and target BGs in an in vitro cell model and an intracranial glioma hormonal mouse model. The photothermal killing effect and tumor targeting effect of this biological PGF on BG cells were evaluated in an in vitro cell model and an intracranial glioma hormonal mouse model by systematically applying Western-blot, qPCR, luciferase activity assay, histopathological detection, transmission electron microscopy. This study employs immunocolloidal gold technology and small animal luciferase in vivo imaging to develop minimally invasive and precise eradication methods for BG. The text has been revised to adhere to the desired characteristics of objectivity, comprehensibility, conventional structure, clear and objective language, format, formal register, structure, balance, precise word choice, and grammatical correctness. The photothermal properties of CdTeSe/ZnS QDs in contact with U251 and U87 cells are observed. Cytotoxicity and luminescence of RAW264.7 after 48 h of co-culture with optimized QDs at different concentration provided the evidence of quantum dots into cellular capacity. Transmission electron microscopy and the flow cytometry detecting suggest that the photothermal effect of quantum dots has a significant killing effect on U87 cells, with greater toxicity and intensity. In short, an effective method for killing gliomas has been achieved, which could contribute to the treatment of human gliomas. This work is to provide direction and experimental basis for finding the precise eradication method of BG. Additionally, a solution based on the micro-nano semiconductor optical device for the photothermal treatment focusing on tumor cells of different stage curing.

Acknowledgements

This work was supported by the Natural Science Foundation of China (81860538, 32360175, 62305262) and the Natural Science Foundation of Ningxia Province (2022AAC03560), Sponsored by Beijing Nova Program (20220484218). Natural Science Foundation of Shaanxi Province (2022JQ-652). Shaanxi Fundamental Science Research Project for Mathematics and Physics (22JSQ026).

Conflicts of interest

There are no conflicts to declare.

Reference

[1] Bush N A O, Chang S M, Berger M S. Current and future strategies for treatment of glioma[J]. Neurosurgical review, 2017, 40:1-14.

[2] Chen W. Q., Zheng R. S., Baade P. D., Zhang S. W., Zeng H. M., Bray F., Jemal A., Yu X. Q., He J. Cancer statistics in China, 2015[J]. CA Cancer J Clin. 2016, 66(2):115-32.

[3] Davis ME. Epidemiology and Overview of Gliomas[J]. Semin Oncol Nurs. 2018; 34(5): 420-429.

[4] Przybylowski CJ, Hervey-Jumper SL, Sanai N. Surgical strategy for insular glioma[J]. J Neurooncol. 2021;151(3):491-497.

[5] Gerwien, A, Mayer, P & Dube, H. Green lightpowered molecular state motor enabling eight-shaped unidirectional rotation. Nat. Commun. 104449(2019)

[6] F. et al. Neurotransmitter-derived lipidoids (NT-lipidoids) for enhanced brain delivery through intravenous injection. Sci. Adv.6, eabb4429 (2020).

[7] Ban Qingfu, Bai Ting, Duan Xiao, Kong Jie. Noninvasive photothermal cancer therapy nanoplatforms via integrating nanomaterials and functional polymers[J]. Biomaterials Science, 2017,5(2):190-210.

[8] Zou Lili, Wang Hong, He Bin, Zeng Lijuan, Tan Tao, Cao Haiqiang, He Xinyu, Zhang Zhiwen, Guo Shengrong, Li Yaping. Current Approaches of Photothermal Therapy in Treating Cancer Metastasis with Nanotherapeutics[J]. Theranostics, 2016,6(6):762-772.

[9] Ngo DN, Ho VTTX, Kim G, Song MS, Kim MR, Choo J, Joo SW, Lee SY. Raman Thermometry Nanopipettes in Cancer Photothermal Therapy[J]. Anal Chem. 2022,94(17):6463-6472.

[10] Yun, S., Kwok, S. Light in diagnosis, therapy and surgery[J]. Nature Biomedical Engineering, 2017,1: 0008.

[11] Li Xingshu, Lovell Jonathan F, Yoon Juyoung, Chen Xiaoyuan. Clinical development and potential of photothermal and photodynamic therapies for cancer[J]. Nature Reviews Clinical Oncology, 2020, 17: 657-674.

[12] Yun, S., Kwok, S. Light in diagnosis, therapy and surgery. Nature Biomedical Engineering, 2017,1, 0008.

[13] Li, X., Lovell, J.F., Yoon, J. et al. Clinical development and potential of photothermal and photodynamic therapies for cancer [J]. ***Nature Reviews Clinical Oncology***, 2020, 17, 657–674.

[14] Victor I Klimov, Ivanov Sergei A, Nanda Jagjit, Achermann Marc, Bezel Ilya, McGuire John A, Piryatinski Andrei. Single-exciton optical gain in semiconductor nanocrystals [J]. Nature, 2007, 447(7143): 441-446.

[15] Hartland G V. Optical studies of dynamics in noble metal nanostructures [J]. Chemical Reviews, 2011,111:3858-3887.

[16] Lin P, Xue Y, Mu X, et al. Tumor Customized 2D Supramolecular Nanodiscs for Ultralong Tumor Retention and Precise Photothermal Therapy of Highly Heterogeneous Cancers [J]. Small.

[17] Wang, Jin, Su Xueqiong, Zhao, PengXiang, Gao, Dongwen, Chen, Ruixiang and Wang, Li. Cancer photothermal therapy based on near infrared fluorescent CdSeTe/ZnS quantum dots [J]. Analytical Methods, 2021, 13(45): 5509-5515.

[18] Lange, N., Szlasa, W., Saczko, J. Chwitkowska, A Potential of cyanine deriveddyes in photodynamic therapy. Pharmaceutics13,818 (2021).

[19] Zhenluan Xue,a Xiaolong Li,a Youbin Li,a Mingyang Jiang,a Guozhong Ren,b Hongrong Liu,a Songjun Zeng *a and Jianhua Hao*c . A 980nm laser-activated upconverted persistent probe for NIR-to-NIR rechargeable in vivo bioimaging [J]. Nanoscale,2017.9 (21):7276-7 283.

[20] Li,H, Tan,ML, Wang,X, Li,F, Zhang,YQ, Zhao,LL, Yang,CH, Chen,GY, Temporal multiplexed in vivo upconversion imaging [J]. Journal of the American Chemical Society,2020.142 (4):2023-2030.

[21] Lötvall J, Hill A F, Hochberg F, et al. Minimal experimental requirements for definition of extracellular vesicles and their functions: a position statement from the International Society for Extracellular Vesicles[J]. Journal of extracellular vesicles, 2014, 3(1): 26913.

[22] Skotland, T., Iversen, T. G., Llorente, A. & Sandvig, K. Biodistribution, pharmacokinetics and excretion studies of intravenously injected

nanoparticles and extracellular vesicles: possibilities and challenges. Adv. Drug Deliv. Rev. 186, 114326 (2022).

[23] Huang, H., Feng, W., Chen, Y. & Shi, J. L. Inorganic nanoparticles in clinical trials and translations. Nano Today 35, 100972 (2020).

[24] Chen Rui-xiang, Su Xue-qiong, Wang Jin, Gao Dong-wen, Pan Yong, Wang Li. Modulation of photoluminescence intensity by surface defects of MAPbBr3 crystals[J]. Optical Materials, 2023,138: 113561.

[25] Y.Gan, et al. Thermal conductivity of GexSb(As)ySe1oo-x-yglasses measured by Raman scattering spectra [J]. J.Raman Spectrosc.2014,45,377-382.

[26] Ayala-Orozco, C., Galvez-Aranda, D., Corona, A. et al. Molecular jackhammers eradicate cancer cells by vibronic-driven action. Nat. Chem. (2023).

[27] Yang, G. et al. A hypoxia-responsive albumin-based nanosystem for deep tumor penetration and excellent therapeutic efficacy. Adv. Mater. 31, e1901513 (2019).

[28] Lange, N., Szlasa, W., Saczko, J.&Chwitkowska, A Potential of cyanine deriveddyes in photodynamic therapy. Pharmaceutics13,818(2021).

[29] Yang,J.-P & Callender RH.The resonanceRaman spectra of some cyanine dyes.J. RamanSpectrosc.16,319-321(1985).

[30] Cui, Y.et al.Molecular plasmon-phononcoupling.Nano Lett.16, 6390-6395(2016)

[31] Kong, F. F et al. Probing intramolecularvibronic coupling through vibronic-stateimaging.Nat. Commun.12, 1280 (2021).

Supplementary Files

This is a list of supplementary files associated with this preprint. Click to download.

- SupportingInformation.pdf